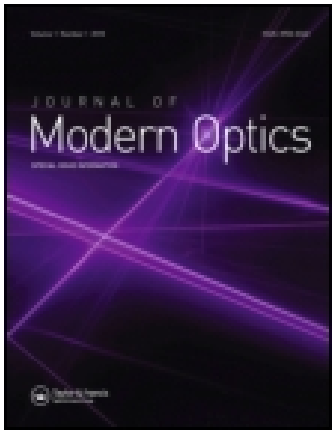

Journal of Modern Optics
Publication details, including instructions for authors and subscription information:
http://www.tandfonline.com/loi/tmop20

Tunneling control of cavity linewidth narrowing via quantum interference in triangular quantum dot molecules

Si-Cong Tian[a], Ren-Gang Wan[b], En-Bo Xing[ac], Cun-Zhu Tong[a] & Yong-Qiang Ning[a]

[a] State Key Laboratory of Luminescence and Applications, Changchun Institute of Optics, Fine Mechanics and Physics, Chinese Academy of Sciences, Changchun, China

[b] State Key Laboratory of Transient Optics and Photonics, Xi'an Institute of Optics and Precision Mechanics, Chinese Academy of Sciences, Xi'an, China

[c] Graduate School of the Chinese Academy of Sciences, Beijing, China

Published online: 22 Jul 2014.

To cite this article: Si-Cong Tian, Ren-Gang Wan, En-Bo Xing, Cun-Zhu Tong & Yong-Qiang Ning (2014) Tunneling control of cavity linewidth narrowing via quantum interference in triangular quantum dot molecules, Journal of Modern Optics, 61:18, 1479-1485, DOI: 10.1080/09500340.2014.941431

To link to this article: http://dx.doi.org/10.1080/09500340.2014.941431

Journal of Modern Optics, 2014
Vol. 61, No. 18, 1479–1485, http://dx.doi.org/10.1080/09500340.2014.941431

Tunneling control of cavity linewidth narrowing via quantum interference in triangular quantum dot molecules

Si-Cong Tian[a]*, Ren-Gang Wan[b], En-Bo Xing[a,c], Cun-Zhu Tong[a]* and Yong-Qiang Ning[a]

[a]*State Key Laboratory of Luminescence and Applications, Changchun Institute of Optics, Fine Mechanics and Physics, Chinese Academy of Sciences, Changchun, China;* [b]*State Key Laboratory of Transient Optics and Photonics, Xi'an Institute of Optics and Precision Mechanics, Chinese Academy of Sciences, Xi'an, China;* [c]*Graduate School of the Chinese Academy of Sciences, Beijing, China*

(*Received 19 June 2014; accepted 30 June 2014*)

A scheme for tunneling control of cavity linewidth narrowing by quantum interference in triangular-type triple quantum dots (TQDs) is proposed. In such system, quantum interference induced by tunneling between the TQDs can result in the appearance of two transparency windows and a steep dispersion. Furthermore, when the sample is embedded in a ring cavity, an ultranarrow transmission peak is obtained within the narrowed transparency windows. And by varying the tunneling, the linewidth and the position of the ultranarrow transmission peak can be engineered. Because no coupling laser is required, the scheme proposed here is more convenient for future experiments and applications in optics, and may be useful in designing novel optoelectronic devices.

Keywords: triple quantum dots; quantum interference; electromagnetically induced transparency; cavity transmission spectrum; linewidth narrowing

1. Introduction

The phenomenon of electromagnetically induced transparency (EIT), which results from quantum interference and coherence [1], plays an important role in the interaction between light and matter [2,3]. Possible applications of EIT include light propagation control [4,5], light storage [6], enhancement of nonlinearity at low light levels [7], etc. Reduced absorption and steep dispersion produced by EIT can induce cavity linewidth narrowing, which is known as intracavity EIT termed by Lukin et al. [8], and may be used for higher solution spectroscopic measurements and frequency stabilization. Cavity linewidth narrowing was experimentally first observed in a hot atomic vapor [9], then in a cold atomic system [10], and in a Doppler-broadened medium [11].

The above studies are carried out in atomic medium, and coupling lasers are essential in these systems. On the other hand, two or more quantum dots coupled by tunneling can form quantum dot molecules, where the tunneling of electrons or holes can be controlled by an external electric field, creating a multilevel structure of excitonic states. Experimentally, double quantum dots (DQDs) have been realized in both vertical [12] and lateral [13] types, and have been used for optical spectroscopy [14], excitonic entanglement [15], single photon and spin storage [16], and coherent population trapping [17]. On the theoretical side, many works have been carried out about DQDs, such as EIT and slow light [18–20], entanglement [21–24], optical bistability [25,26], coherent population transfer [27], narrowing of transmission spectrum [28], and fluorescence spectrum [29].

Recently, a four-level tripod atomic system has been extensively investigated to EIT and slow light [30,31], control of spontaneous emission [32], stimulated Raman adiabatic passage [33], two-dimensional atom localization [34,35], cavity linewidth narrowing [36,37], and so on. Building on DQDs, triple quantum dots (TQDs) have been achieved in much experimental progress [38–41]. And with tunneling coupling, triangular-type TQDs can form a four-level tripod system. And in such triangular-type TQDs, two tunneling between the dots can produce quantum interference, which has been used for slow light [42] and optical bistability [43]. Inspired by these works, in this paper, we propose a scheme for obtaining a tunable ultranarrow cavity transmission in triangular TQDs. In such system, quantum interference can be produced by tunneling coupling, resulting in two transparency windows. By tuning the tunneling, the transparency windows can be made very narrow, and within the narrowed transparency window, an ultranarrow cavity transmission can be obtained. Here, we use tunneling instead of coupling lasers to obtain cavity linewidth narrowing, which makes the scheme be more convenient for experiments and applications in optics.

*Corresponding authors. Email: tiansicong@ciomp.ac.cn; tongcz@ciomp.ac.cn

2. Model and equations

The schematic of the setup of a triangular TQDs is shown in Figure 1(*a*). Because of the nanoscale interdot separation, the electron states in QDs are delocalized, while the hole states in QDs are localized. And the tunneling between the dots can be controlled by placing a gate electrode between QDs. In the absence of a bias voltage, the electron tunneling between QD1 and QD2, and that of between QD1 and QD3 are very weak. While in the presence of a bias voltage, the band profiles' alignment is modified, resulting in the enhancement of the electron tunneling between QD1 and QD2, and QD1 and QD3. And in both cases, there is no tunneling between QD2 and QD3. We show the schematic of the level configuration of the TQDs in Figure 1(*b*). Without the optical excitation, there is no exciton inside all the QDs, condition represented by the state $|0\rangle$. Then with the optical excitation, a direct exciton is created inside QD1, which corresponds to state $|1\rangle$. The tunneling can allow the electron to tunnel from QD1 to QD2 or QD3 forming the indirect excitons, which are denoted as state $|2\rangle$ and state $|3\rangle$, respectively.

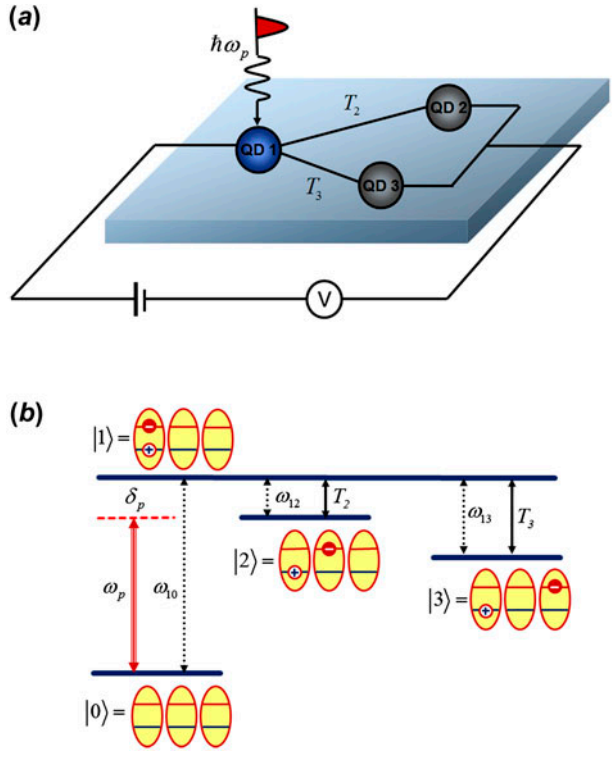

Figure 1. (*a*) The schematic of the setup of triangular TQDs. The probe field transmits the QD 1. V_B is a bias voltage. (*b*) The schematic of the level configuration of triangular TQDs. (The colour version of this figure is included in the online version of the journal.)

The Hamiltonian of these TQDs in the interaction picture and in the rotating wave and dipole approximations is given by (assumption of $\hbar = 1$)

$$H = \sum_{j=0}^{3} E_j|j\rangle\langle j| + [(\Omega_p e^{-i\omega_p t}|0\rangle\langle 1| + T_2|2\rangle\langle 1| + T_3|3\rangle\langle 1|) + \text{H.c.}], \quad (1)$$

where $E_j = \hbar\omega_j$ is the energy of state $|j\rangle$, ω_p is the probe field frequency, $\Omega_p = \mu_{01}\cdot e\cdot E$ is the Rabi frequency of the transition $|0\rangle \rightarrow |1\rangle$, with μ_{01} being the associated dipole transition-matrix element, **e** is the polarization vector, and E is the electric-field amplitude of the laser pulse. And T_2 and T_3 are the tunneling coupling between states $|1\rangle$ and $|2\rangle$, and states $|1\rangle$ and $|3\rangle$, respectively.

To remove the time-dependent oscillatory terms, the unitary transformation is used [44],

$$U = \exp\left[\frac{i\omega_p t}{2}(|1\rangle\langle 1| + |2\rangle\langle 2| + |3\rangle\langle 3|)\right]. \quad (2)$$

Then using Baker–Hausdorff lemma [45], Equation (1) can be written as follows,

$$H = \begin{pmatrix} -\delta_p & \Omega_p & 0 & 0 \\ \Omega_p & \delta_p & T_2 & 0 \\ 0 & T_2 & \delta_2 & T_3 \\ 0 & 0 & T_3 & \delta_3 \end{pmatrix}. \quad (3)$$

Here, $\delta_p = \omega_{10} - \omega_p$ is the detuning of the probe field, with ω_{10} being the transition frequency between $|1\rangle$ and $|0\rangle$ states. And other detunings are denoted as $\delta_2 = \delta_p + 2\omega_{12}$, $\delta_3 = \delta_p + 2\omega_{13}$, with ω_{12} and ω_{13} as the energy splitting of states $|1\rangle$ and $|2\rangle$, and that of states $|1\rangle$ and $|3\rangle$, respectively. Experimentally, ω_{12} and ω_{13} can be modified by manipulation of the external electric field that changes the effective confinement potential.

The dynamics of the system is described by Liouville–von Neumman–Lindblad equation [46]

$$\frac{d\rho}{dt} = -\frac{i}{\hbar}[H, \rho(t)] + L(\rho), \quad (4)$$

where $\rho(t)$ is the density-matrix operator. The Liouville operator $L(\rho)$ describes the dissipative process. With the Markovian approximation, Liouville operator can be written as [47]

$$L(\rho) = \frac{1}{2}\sum_i \Gamma_{ij}(2|j\rangle\langle i|\rho|i\rangle\langle j| - \rho|i\rangle\langle i| - |i\rangle\langle i|\rho) + \gamma_{i0}{}^d(2|i\rangle\langle i|\rho|i\rangle\langle i| - \rho|i\rangle\langle i| - |i\rangle\langle i|\rho), \quad (5)$$

where Γ_{ij} is the radiative decay rate of populations from $|i\rangle \rightarrow |j\rangle$ and $\gamma_{i0}{}^d$ is the pure dephasing rates.

Substituting Equations (3) and (5) into Equation (4), the density matrix ρ_{ij} elements are

$$\dot{\rho}_{01} = -i[\Omega_p(\rho_{11} - \rho_{00}) + T_2\rho_{02} + T_3\rho_{03}] + (i\delta_p - \gamma_1)\rho_{01}, \tag{6a}$$

$$\dot{\rho}_{02} = -i(T_2\rho_{01} - \Omega_p\rho_{12}) + \left[\frac{i}{2}(\delta_p + \delta_2) - \gamma_2\right]\rho_{02}, \tag{6b}$$

$$\dot{\rho}_{03} = -i(T_3\rho_{01} - \Omega_p\rho_{13}) + \left[\frac{i}{2}(\delta_p + \delta_3) - \gamma_3\right]\rho_{03}, \tag{6c}$$

$$\dot{\rho}_{11} = -i\left[\Omega_p(\rho_{10} - \rho_{01}) + T_2(\rho_{12} - \rho_{21}) + T_3(\rho_{13} - \rho_{31})\right] - \Gamma_{10}\rho_{11}, \tag{6d}$$

$$\dot{\rho}_{12} = -i\left[T_2(\rho_{11} - \rho_{22}) - \Omega_p\rho_{02} - T_3\rho_{32}\right] + \left[\frac{i}{2}(\delta_2 - \delta_p) - (\gamma_1 + \gamma_2)\right]\rho_{12}, \tag{6e}$$

$$\dot{\rho}_{13} = -i\left[T_3(\rho_{11} - \rho_{33}) - \Omega_p\rho_{03} - T_2\rho_{23}\right] + \left[\frac{i}{2}(\delta_3 - \delta_p) - (\gamma_1 + \gamma_3)\right]\rho_{13}, \tag{6f}$$

$$\dot{\rho}_{22} = -iT_2(\rho_{21} - \rho_{12}) - \Gamma_{20}\rho_{22}, \tag{6g}$$

$$\dot{\rho}_{23} = -i(T_3\rho_{21} - T_2\rho_{13}) + \left[\frac{i}{2}(\delta_3 - \delta_2) - (\gamma_2 + \gamma_3)\right]\rho_{23}, \tag{6h}$$

$$\dot{\rho}_{33} = -iT_3(\rho_{31} - \rho_{13}) - \Gamma_{30}\rho_{33}, \tag{6i}$$

with $\rho_{00} + \rho_{11} + \rho_{22} + \rho_{33} = 1$ and $\dot{\rho}_{ij} = \dot{\rho}_{ji}$. And $\gamma_i = \frac{1}{2}\Gamma_{i0} + \gamma_{i0}{}^d (i = 1 - 3)$ is the typical effective decay rate.

In the limit of a weak probe field, almost all excitons will remain in state $|0\rangle$ and hence, we may assume that $\rho_{00} = 1$ and for other elements, $\rho_{ij} = 0$ for the steady state. Then we can obtain the expression of ρ_{01} by solving Equation (6),

$$\rho_{01} = \frac{1}{(\delta_p - i\gamma_1) - \frac{T_2{}^2}{(\delta_p + \omega_{12} - i\gamma_2)} - \frac{T_3{}^2}{(\delta_p + \omega_{13} - i\gamma_3)}} \tag{7}$$

And the probe susceptibility χ is proportional to the density matrix element ρ_{01},

$$\chi(\delta_1) = \frac{N|\mu_{01}|^2}{\varepsilon_0\Omega_p} \frac{1}{(\delta_p - i\gamma_1) - \frac{T_2{}^2}{(\delta_p + \omega_{12} - i\gamma_2)} - \frac{T_3{}^2}{(\delta_p + \omega_{13} - i\gamma_3)}} \tag{8}$$

Here, $N = (\Gamma/V)$ is the excitons volume density, with Γ being the optical confinement factor, V being the volume of the TQDs, and ε_0 is the dielectric constant [48].

The susceptibility χ can be separated into real (χ') and imaginary (χ'') parts, which represent the absorption and dispersion of the medium, respectively.

3. Absorption and dispersion spectrum of TQDs

In this part, we plot in Figure 2 the absorption (χ'') and dispersion (χ') spectrum according to Equation (8) for different parameters. We point out that the absorption and dispersion spectra have been studied in an atomic system with the coupling lasers. But here, we use tunneling instead of the coupling lasers and obtain similar results. And in TQDs, the tunneling coupling T_2

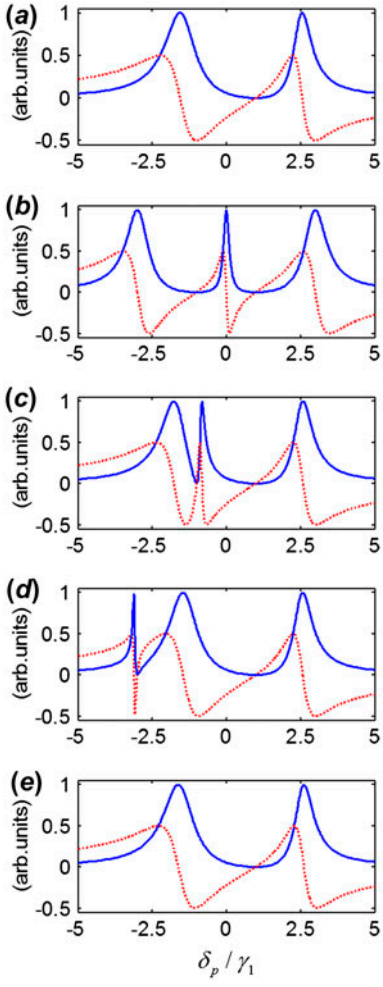

Figure 2. The absorption spectrum (solid line) and dispersion spectrum (dotted line) as a function of δ_p. The parameters are (*a*) $T_2 = 2$, $T_3 = 0$, $\omega_{12} = -1$, $\omega_{13} = 0$, (*b*) $T_2 = 2$, $T_3 = 2$, $\omega_{12} = -1$, $\omega_{13} = 1$, (*c*) $T_2 = 2$, $T_3 = 0.5$, $\omega_{12} = -1$, $\omega_{13} = 1$, (*d*) $T_2 = 2$, $T_3 = 0.5$, $\omega_{12} = -1$, $\omega_{13} = 3$, and (*e*) $T_2 = 2$, $T_3 = 0.5$, $\omega_{12} = -1$, $\omega_{13} = -1$. Other parameters are $\Gamma_{10} = 0.66$, $\Gamma_{20} = \Gamma_{30} = 10^{-4}\Gamma_{10}$, $\gamma_1 = 1$, and $\gamma_2 = \gamma_3 = 10^{-3}\gamma_1$. And all the parameters are scaled by γ_1. (The colour version of this figure is included in the online version of the journal.)

and T_3 depend on the barrier characteristics and the external electric field. Energy splitting ω_{12} and ω_{13} can be done by manipulation of the external electric field that changes the effective confinement potential. In addition, in this investigation we work in the low temperature regime, and consider both the population decay rates and the dephasing rates. The realistic values of the parameters are according to Ref. [19] and Refs. therein [49–56]. And for simplicity, all the parameters are scaled by the decay rate γ_1. Though some of the values of parameters are for DQDs, it can be inferred that the tunneling, energy splitting and decay rates of TQDs have the same values with that of DQDs.

Here, we consider the case that the tunneling T_2 and energy splitting ω_{12} are not changed, and see how T_3 and ω_{13} modify the absorption and dispersion spectra. First, when only QD 1 and QD 2 are coupled together by tunneling T_2, the system reduces to DQDs and the results in Figure 2(*a*) are similar to the earlier work [18,19]. Then in Figure 2(*b*)–(*e*), we show the case that QD 3 is also coupled to the system by tunneling T_3. In this case, the electron can tunnel from QD 1 to QD 2 or QD 3, forming the four-level tripod system. When $\omega_{13}=-\omega_{12}$ and $T_3=T_2$, the absorption spectrum is symmetrical, and two wide transparency windows appear (solid line in Figure 2(*b*)). Within the two transparency windows, the slope of the dispersion is the same (dotted line in Figure 2(*b*)). With decreasing value of T_3, the absorption spectrum becomes unsymmetrical with one transparency window being much narrower than the other one, and the dispersion within the narrower transparency window is much steeper (Figure 2(*c*)). Then we tune the energy splitting ω_{13}. With increase in the value of ω_{13}, the position of the narrower transparency window moves to the blue frequency side, and the dispersion within the narrower transparency window is steeper as well, as shown in Figure 2(*d*). And last, we show a special case of $\omega_{13}=\omega_{12}$ in Figure 2(*e*). As one can see, there is only one wide transparency window in the absorption spectrum with gentle dispersion in the area of the transparency window.

To obtain a more general case, we plot in Figure 3, the three-dimensional absorption and dispersion spectra for various values of tunneling T_3 and energy splitting ω_{13}. From Figure 3(*a*) and (*b*), one can see that there are two transparency windows locating at the position of $\delta_p=-\omega_{12}$ and $\delta_p=-\omega_{13}$ under the coupling of both tunneling. And the decreasing intensity of tunneling T_3 can result in the narrowing width of the transparency window, as show in Figure 3(*a*). This narrowed

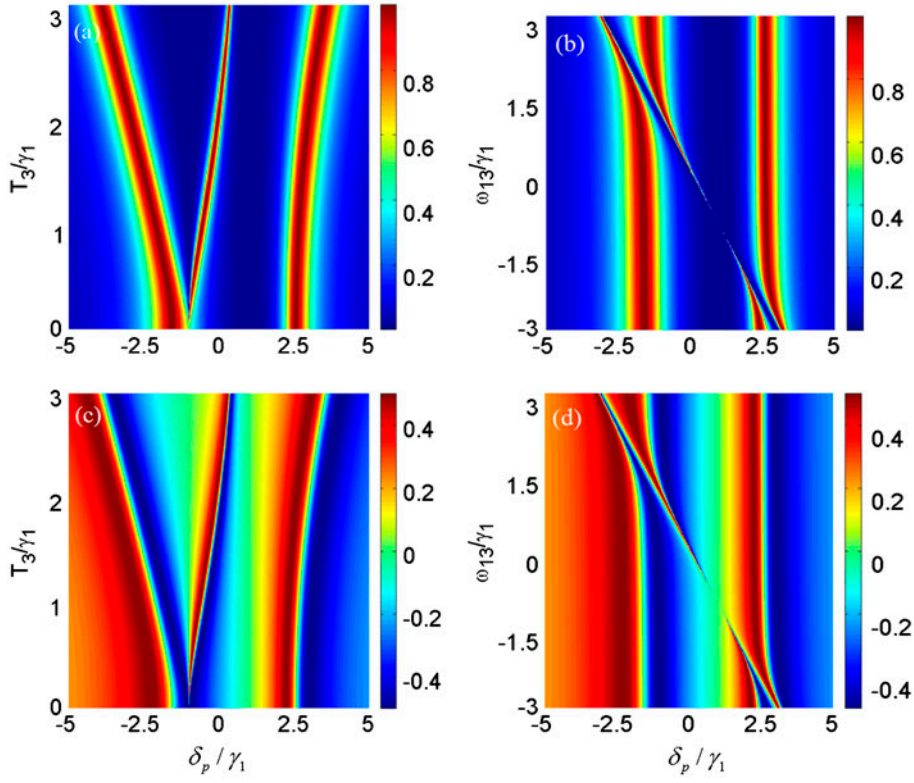

Figure 3. (*a*) The absorption and (*c*) dispersion spectra as functions of δ_p and T_3. (*b*) The absorption and (*d*) dispersion spectra as functions of δ_p and ω_{13}. Other parameters are the same as those in Figure 2. (The colour version of this figure is included in the online version of the journal.)

transparency window can occur in large range of ω_{13}, as long as $\omega_{13} \neq \omega_{12}$ (Figure 3(*b*)). And within the narrowed transparency window, steep dispersion can be obtained (Figure 3(*c*) and (*d*)).

From Figures 2 and 3, we can conclude that the intensity of the tunneling coupling can modify the width of the transparency windows, while the energy splitting can change the position of them. And in the area of the narrower transparency window, much steeper dispersion can be obtained. On the other hand, the changing of value of T_2 and ω_{12} can also modify the absorption and dispersion spectra. Because of the symmetrical setup, the results are similar to the above (we do not show these results here).

4. Transmission spectrum of TDQs

In this part, we embed the TQDs sample in a ring cavity, as shown in Figure 4. We consider the optical cavity of length L with TQDs sample of length l. Then the cavity transmission can be expressed as [8]

$$(\omega) = \frac{t^2}{1 + r^2\kappa^2 - 2r\kappa\cos[\Phi(\omega)]}, \tag{9}$$

Here, t and r denote the transmissivity and the reflectivity of both the input and the output mirrors with $r^2 + t^2 = 1$. For simplicity, we assume that mirror 3 has 100% reflectivity. And $\Phi(\omega) = \frac{\omega}{c}(L + l\chi')$ is the total phase shift, which is contributed by the real part (χ') of the susceptibility of the TQDs. And $\kappa = \exp(-\frac{\omega}{c}l\chi'')$ is the medium absorption per round trip, which is caused by the imaginary part (χ'') of the susceptibility of the TQDs, leading to the attenuation of the amplification of the probe field.

On inspection of the round-trip phase shift, the pulling equation representing the resonance frequency of the combined cavity and medium system is [8]

$$\omega_r = \frac{1}{1+\eta}\omega_c + \frac{\eta}{1+\eta}\omega_p, \tag{10a}$$

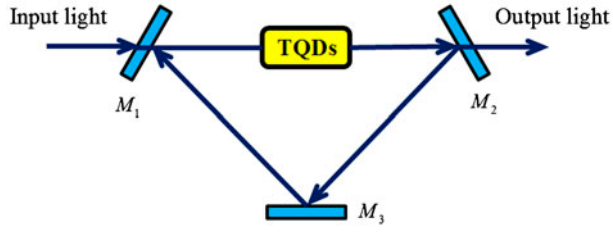

Figure 4. The schematic of a cavity TQDs system. (The colour version of this figure is included in the online version of the journal.)

$$\eta = \omega_p \frac{l}{2L}\frac{\partial\chi'}{\partial\omega_p} \tag{10b}$$

Here, η defines a frequency-locking or stabilization coefficient, which is relative to the dispersion of the system. Equation (10) indicates that ω_r is contributed by two factors, one is the resonance frequency of the empty cavity ω_c, with $\omega_c = mc/L$ (for integer m) and the other is the probe transition frequency of TQDs. When EIT is induced in TQDs medium, the probe transition frequency ω_p is close to ω_{10}. Therefore, the medium around transparency window will pull the resonance frequency ω_r to its respective EIT frequency.

Using the same methods in Ref. [8], the width of cavity resonances $\delta\omega$ changed by the intracavity medium is

$$\delta\omega = \frac{1 - r\kappa}{\sqrt{\kappa}(1-r)}\frac{1}{1-\eta}\delta\omega_c, \tag{11}$$

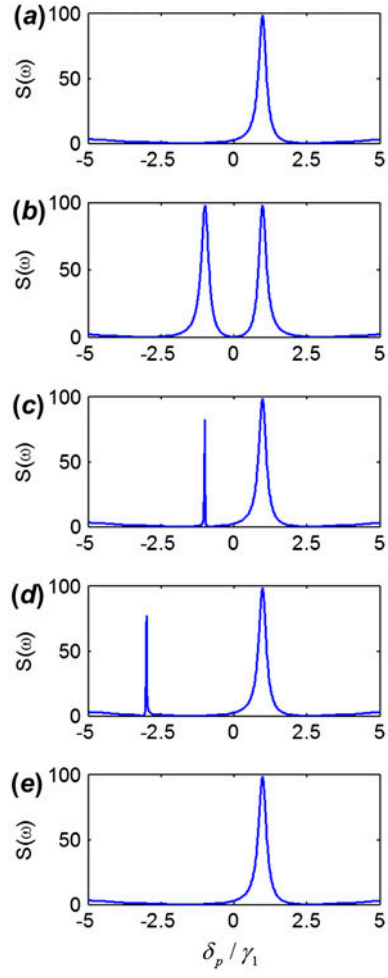

Figure 5. The cavity transmission spectrum as a function of δ_p. The parameters refer to Figure 2, and $r = 0.98$. (The colour version of this figure is included in the online version of the journal.)

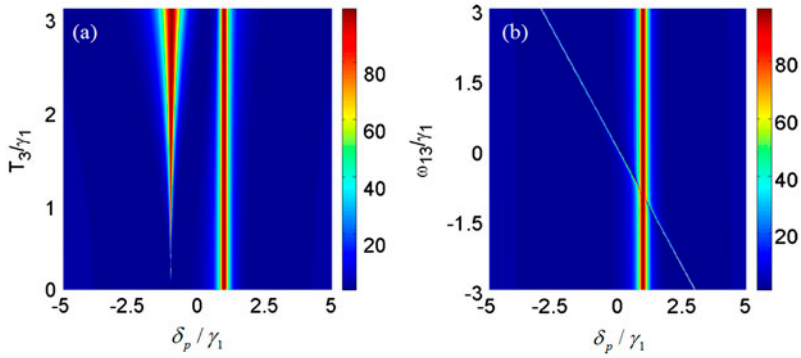

Figure 6. (*a*) The cavity transmission spectrum as functions of δ_p and T_3. (*b*) The cavity transmission spectrum as functions of δ_p and ω_{13}. The parameters refer to Figure 2, and $r = 0.98$. (The colour version of this figure is included in the online version of the journal.)

where $\delta\omega_c$ is the empty cavity linewidth. And $(1 - r\kappa)/\sqrt{\kappa}(1 - r)$ describes an enhancement of the effective cavity and medium width due to additional losses, while $1/(1-\eta)$ describes the reduction due to the linear dispersion. When EIT is induced, the absorption can be negligible ($\chi'' \to 0$), whereas, if the dispersion is large, then Equation (11) can be simplified as

$$\delta\omega = \frac{1}{1-\eta}\delta\omega_c. \tag{12}$$

Equation (12) indicates that the large dispersion will result in substantial line narrowing within the transparency windows.

According to Equation (9), we plot the numerical simulation of the cavity transmission spectrum in Figure 5 with the same parameters used in Figure 2. First, in the absence of T_3, the system is similar to DQDs and one broad transmission peak appears, as shown in Figure 5(*a*). The dispersion in Figure 2(*a*) is gentle, which is responsible for the broad linewidth of the transmission peak. Then we apply both tunneling T_2 and T_3 and create a four-level tripod system. When $\omega_{13} = -\omega_{12}$ and $T_3 = T_2$, one can see that the transmission spectrum is symmetrical with two same wide transmission peaks, as shown in Figure 5(*b*). With decreasing intensity of tunneling T_3, the transmission peak close to $\delta_p = -\omega_{13}$ becomes much narrower than the one close to $\delta_p = -\omega_{12}$, but keep the position unchanged (Figure 5(*c*)). Then we increase the energy splitting of ω_{13}, compared with Figure 5(*c*), the narrower transmission peak moves to the blue frequency side, as shown in Figure 5(*d*). The narrowing of the transmission peak is due to the steeper dispersion within the narrower transparency window (Figure 2(*c*) and (*d*)). And finally when $\omega_{13} = \omega_{12}$, the extra narrow transmission peak disappears, and there is only one wide transmission peak in the spectrum (Figure 5(*e*)). This is because, for $\omega_{13} = \omega_{12}$, only one wide transparency window is obtained (Figure 2(*e*)).

The transmission spectrum as functions of δ_p and T_3 is shown in Figure 6(*a*). As can be seen, with decreasing value of T_3, the linewidth of the transmission peak close to $\delta_p = -\omega_{13}$ is decreased, while that of close to $\delta_p = -\omega_{12}$ is nearly unchanged. We showed in Figure 6(*b*) the transmission spectrum as functions of δ_p and ω_{13}, and find that there is always one narrow transmission peak close to $\delta_p = -\omega_{13}$. From Figures 5 and 6, the conclusion can be made that the intensity of tunneling can modify the linewidth of the transmission peak, and the energy splitting can change the position of it. And this can be done by changing the external electric field in TQDs.

5. Conclusions

In conclusion, we have proposed a scheme for obtaining a tunable ultranarrow cavity transmission controlled by tunneling in triangular TQDs. Due to quantum interference produced by tunneling between the dots, two transparency windows are obtained. By proper tuning the tunneling, the transparency window can be made very narrow, and within the narrow transparency window, high dispersion can be acquired. Furthermore, when the sample is embedded in a ring cavity, ultranarrow transmission peaks are obtained. And the linewidth and the position of this ultranarrow transmission peak can be controlled by adjusting the tunneling. Such cavity linewidth narrowing is due to the steep dispersion and reduced absorption produced by the tunneling, and may be used in the area of higher solution spectroscopic measurements and frequency stabilization.

Funding

This work is supported by the National Basic Research Program of China [grant number 2013CB933300]; the National Natural Science Foundation of China [grant number

11304308], [grant number 61176046]; Jilin Provincial Natural Science Foundation [grant number 20140101203JC]; the Hundred Talents Program of Chinese Academy of Sciences.

References

[1] Ficek, Z.; Swain, S. *Quantum Interference and Coherence: Theory and Experiments*; Springer: New York, 2004.
[2] Harris, S.E. *Phys. Today* **1997,** *50,* 36–42.
[3] Fleischhauer, M.; Imamoglu, A.; Marangos, J.P. *Rev. Modern Phys.* **2005,** *77,* 633–673.
[4] Hau, L.V.; Harris, S.E.; Dutton, Z.; Behroozi, C.H. *Nature* **1999,** *397,* 594–598.
[5] Kash, M.M.; Sautenkov, V.A.; Zibrov, A.S.; Hollberg, L.; Welch, G.R.; Lukin, M.D.; Rostovtsev, Y.; Fry, E.S.; Scully, M.O. *Phys. Rev. Lett.* **1999,** *82,* 5229–5232.
[6] Fleischhauer, M.; Lukin, M.D. *Phys. Rev. Lett.* **2000,** *84,* 5094–5097.
[7] Harris, S.E.; Hau, L.V. *Phys. Rev. Lett.* **1999,** *82,* 4611–4614.
[8] Lukin, M.D.; Fleischhauer, M.; Scully, M.O.; Velichansky, V.L. *Opt. Lett.* **1998,** *23,* 295–297.
[9] Wang, H.; Goorskey, D.J.; Burkett, W.H.; Xiao, M. *Opt. Lett.* **2000,** *25,* 1732–1734.
[10] Hernandez, G.; Zhang, J.P.; Zhu, Y.F. *Phys. Rev. A: At. Mol. Opt. Phys.* **2007,** *76,* 053814.
[11] Wu, H.; Gea-Banacloche, J.; Xiao, M. *Phys. Rev. Lett.* **2008,** *100,* 173602.
[12] Xie, Q.H.; Madhukar, A.; Chen, P.; Kobayashi, N.P. *Phys. Rev. Lett.* **1995,** *75,* 2542–2545.
[13] Beirne, G.J.; Hermannstädter, C.; Wang, L.; Rastelli, A.; Schmidt, O.G.; Michler, P. *Phys. Rev. Lett.* **2006,** *96,* 137401.
[14] Stinaff, E.A.; Scheibner, M.; Bracker, A.S.; Ponomarev, I.V.; Korenev, V.L.; Ware, M.E.; Doty, M.F.; Reinecke, T.L.; Gammon, D. *Science* **2006,** *311,* 636–639.
[15] Kim, D.; Carter, S.G.; Greilich, A.; Bracker, A.S.; Gammon, D. *Nat. Phys.* **2010,** *7,* 223–229.
[16] Boyer de la Giroday, A.; Sköld, N.; Stevenson, R.M.; Farrer, I.; Ritchie, D.A.; Shields, A.J. *Phys. Rev. Lett.* **2011,** *106,* 216802.
[17] Weiss, K.M.; Elzerman, J.M.; Delley, Y.L.; Miguel-Sanchez, J.; Imamoğlu, A. *Phys. Rev. Lett.* **2012,** *109,* 107401.
[18] Yuan, C.H.; Zhu, K.D. *Appl. Phys. Lett.* **2006,** *89,* 052115.
[19] Borges, H.S.; Sanz, L.; Villas-Bôas, J.M.; Diniz Neto, O.O.; Alcalde, A.M. *Phys. Rev. B: Condens. Matter* **2012,** *85,* 115425.
[20] Michael, S.; Chow, W.W.; Schneider, H.C. *Phys. Rev. B: Condens. Matter* **2013,** *88,* 125305.
[21] Lü, X.Y.; Wu, J.; Zheng, L.L.; Zhan, Z.M. *Phys. Rev. A: At. Mol. Opt. Phys.* **2011,** *83,* 042302.
[22] Cheng, M.T.; Ma, X.S.; Luo, Y.Q.; Wang, P.Z.; Zhao, G.X. *Appl. Phys. Lett.* **2011,** *99,* 223509.
[23] Zheng, A.S.; Cheng, Y.J.; Liu, J.B. *J. Opt. Soc. Am. B: Opt. Phys.* **2013,** *30,* 3168–3173.
[24] Liu, S.P.; Yu, R.; Li, J.H.; Wu, Y. *J. Appl. Phys.* **2014,** *115,* 134312.
[25] Li, J.; Yu, R.; Liu, J.; Huang, P.; Yang, X. *Physica E* **2008,** *41,* 70–73.
[26] Wang, Z.P.; Zhen, S.L.; Wu, X.Q.; Zhu, J.; Cao, Z.G.; Yu, B.L. *Opt. Commun.* **2013,** *304,* 7–10.
[27] Voutsinas, E.; Terzis, A.F.; Paspalakis, E. *Phys. Lett. A* **2014,** *378,* 219–225.
[28] Peng, Y.D.; Niu, Y.P.; Cui, N.; Gong, S.Q. *Opt. Commun.* **2011,** *284,* 824–827.
[29] Tian, S.C.; Tong, C.Z.; Wang, C.L.; Wang, L.J.; Wu, H.; Xing, E.B.; Ning, Y.Q.; Wang, L.J. *Opt. Commun.* **2014,** *312,* 296–301.
[30] Paspalakis, E.; Knight, P.L. *Phys. Rev. A: At. Mol. Opt. Phys.* **2002,** *66,* 015802.
[31] Paspalakis, E.; Knight, P.L. *J. Opt. B: Quantum Semiclass. Opt.* **2002,** *4,* S372–S375.
[32] Wu, J.H.; Li, A.J.; Ding, Y.; Zhao, Y.C.; Gao, J.Y. *Phys. Rev. A: At. Mol. Opt. Phys.* **2005,** *72,* 023802.
[33] Wang, L.; Song, X.L.; Li, A.J.; Wang, H.H.; Wei, X.G.; Kang, Z.H.; Jiang, Y.; Gao, J.Y. *Opt. Lett.* **2008,** *33,* 2380–2382.
[34] Wan, R.G.; Kou, J.; Jiang, L.; Jiang, Y.; Gao, J.Y. *J. Opt. Soc. Am. B: Opt. Phys.* **2011,** *28,* 10–17.
[35] Wang, Z.P.; Yu, B.L. *Laser Phys. Lett.* **2014,** *11,* 035201.
[36] Peng, Y.D.; Jin, L.L.; Niu, Y.P.; Gong, S.Q. *J. Mod. Opt.* **2010,** *57,* 641–645.
[37] Ying, K.; Niu, Y.P.; Chen, D.J.; Cai, H.W.; Qu, R.H.; Gong, S.Q. *J. Opt. Soc. Am. B: Opt. Phys.* **2014,** *31,* 144–148.
[38] Hsieh, C.Y.; Shim, Y.P.; Korkusinski, M.; Hawrylak *Rep. Prog. Phys.* **2012,** *75,* 114501.
[39] Hayne, M.; Provoost, R. *Phys. Rev. B: Condens. Matter* **2000,** *62,* 324–328.
[40] Rainò, G.; Salhi, A.; Tasco, V.; De Vittorio, M.; Passaseo, A.; Cingolani, R.; De Giorgi, M.; Luna, E.; Trampert, A. *J. Appl. Phys.* **2008,** *103,* 096107.
[41] Songmuang, R.; Kiravittaya, S.; Schmidt, O.G. *Appl. Phys. Lett.* **2003,** *82,* 2892–2894.
[42] Tian, S.C.; Tong, C.Z.; Wan, R.G.; Ning, Y.Q.; Wang, L.J. **2013,** arXiv:1310.4599.
[43] Reza Hamedi, H. *Physica B* **2014,** *449,* 5–9.
[44] Villas-Bôas, J.M.; Govorov, A.O.; Ulloa, S.E. *Phys. Rev. B: Condens. Matter* **2004,** *69,* 125342.
[45] Sakurai, J.J. *Modern Quantum Mechanics*; Addison-Wesley; Reading, MA, 1994.
[46] Rau, A.R.P.; Zhao, W. *Phys. Rev. A: At. Mol. Opt. Phys.* **2003,** *68,* 052102.
[47] Villas-Bôas, J.M.; Ulloa, S.E.; Govorov, A.O. *Phys. Rev. B: Condens. Matter* **2007,** *75,* 155334.
[48] Kim, J.; Chuang, S.L.; Ku, P.C.; Chang-Hasnain, C.J. *J. Phys.: Condens. Matter* **2004,** *16,* S3727–S3735.
[49] Bonadeo, N.H.; Erland, J.; Gammon, D.; Park, D.; Katzer, D.S.; Steel, D.G. *Science* **1998,** *282,* 1473–1476.
[50] Kamada, H.; Gotoh, H.; Temmyo, J.; Takagahara, T.; Ando, H. *Phys. Rev. Lett.* **2001,** *87,* 246401.
[51] Tackeuchi, A.; Kuroda, T.; Mase, K. *Phys. Rev. B: Condens. Matter* **2000,** *62,* 1568–1571.
[52] Chen, P.; Piermarocchi, C.; Sham, L.J. *Phys. Rev. Lett.* **2001,** *87,* 067401.
[53] Negoita, V.; Snoke, D.W.; Eberl, K. *Phys. Rev. B: Condens. Matter* **1999,** *60,* 2661–2669.
[54] Borri, P.; Langbein, W.; Woggon, U.; Schwab, M.; Bayer, M.; Fafard, S.; Wasilewski, Z.; Hawrylak, P. *Phys. Rev. Lett.* **2003,** *91,* 267401.
[55] Bardot, C.; Schwab, M.; Bayer, M.; Fafard, S.; Wasilewski, Z.; Hawrylak, P. *Phys. Rev. B: Condens. Matter* **2005,** *72,* 035314.
[56] Butov, L.V.; Zrenner, A.; Abstreiter, G.; Böhm, G.; Weimann, G. *Phys. Rev. Lett.* **1994,** *73,* 304–307.